Hindawi
International Journal of Polymer Science
Volume 2023, Article ID 3892823, 12 pages
https://doi.org/10.1155/2023/3892823

Research Article

Thermal and Dielectric Behaviour of Polymer-Based Nanocomposites Flexible Sheets as Highly Stable Dielectric Materials

S. Pervaiz,[1] N. Kanwal,[1] A. Shahzad,[1] M. Saleem,[2] and I. A. Khan[1]

[1]*Department of Physics, Government College University Faisalabad, Faisalabad 38000, Pakistan*
[2]*Department of Physics, Lahore University of Management Sciences, Lahore 54000, Pakistan*

Correspondence should be addressed to M. Saleem; murtaza.saleem@lums.edu.pk and I. A. Khan; ijazahmad@gcuf.edu.pk

Received 15 April 2022; Revised 1 November 2022; Accepted 2 November 2022; Published 5 January 2023

Academic Editor: Peter Foot

The silica zinc oxide nanoparticles filled poly-vinylidene-fluoride (PVDF)-based nanocomposite flexible sheets (NC FSs) are synthesized by co-precipitation method. The X-ray diffraction patterns reveal the development of various diffraction planes related to zinc oxide (ZnO) and SiO_2 phases. The crystallinity of ZnO phase is decreased with increasing weight percent (wt.%) of silica nanofillers (NFs). The scanning electron microscope microstructure of synthesized PVDF-based NCs FSs is changed with increasing wt.% of silica NFs. The energy-dispersive X-ray spectroscopy and Fourier-transform infrared spectroscopy analyses confirm the presence of different elements and the formation of chemical bonding between them. In high temperature region, the weight-loss of synthesized PVDF-based NCs FSs is decreased from 89.90% to 49.26% with increasing wt.% of silica NFs. The values of dielectric permittivity, loss-factor, impedance, and AC-conductivity of PVDF-based NC FSs synthesized for maximum amount of silica NFs are found to be 13.7, 0.03, 0.16 MΩ, and 19.9×10^{-6} S/m, respectively. Results show that the synthesized PVDF-based NC FSs are the potential candidates of light emitting diodes and energy storage devices.

1. Introduction

Polymer-based nanocomposite flexible sheets (NC FSs) have drawn a huge attention of researchers due to their remarkable industrial applications. The polymer-based NC FSs have enhanced properties as compared to pure polymer, which depend on the concentration and types of nanofillers (NFs), microstructures, and interfacial area of polymer-based NC FSs. These parameters play an important role to enhance the properties of polymer-based NC FSs due to high aspect ratio [1–3]. The various properties of polymer-based NC FSs are associated with the nature and amount of polymer and NFs and their homogeneous mixing during the synthesis process [4, 5]. It is known that the dielectric properties of polymer-based NC FSs depend on size and distribution of NFs. The outstanding properties of polymer matrices are associated with the complex-motion of NFs, which causes a significant change, whereas the polymeric boundaries may act as trapping sites of charge carriers. It is necessary to study the influence of boundaries generation, transportation, and storage of charge carrier within the polymer matrix. The study of dielectric properties of polymer-based NC FSs as a function of increasing frequency is more appropriate to correlate the structural and microstructural features with the dielectric parameters [6]. Poly-vinylidene-fluoride (PVDF) has huge consideration because of remarkable dielectric, mechanical, and chemical properties [7–9]. The dielectric properties of PVDF [10] may be enhanced by mixing it with inorganic material of different sizes [11–13]. The polymer community is using semiconducting materials, such as zinc oxide (ZnO), owing to its remarkable properties as NFs in polymer matrix to synthesize polymer-based NC FSs to improve the optical, electrical, and dielectric properties [14–16]. The size of NFs plays a vital role to enhance the multidimensional properties of polymer-based NC FSs since the NFs increases the surface area [17, 18]. The mixing of silica NFs into polymer matrix also plays a vital role to improve their mechanical and dielectric properties as well

as enhanced the heat and wear resistance [19]. The crystal structure, surface morphologies, and optical properties of polymer-based NC FSs are also depended on the nanoscale dimensions of silica NFs [19–21]. In short, the more detailed information about the optical, electrical, and dielectric properties of polymer-based NC FSs can be found in literature [22–24]. However, more research work related to the synthesis of polymer-based NC FSs is required to develop the linkage between crystal structure, surface morphology, thermal stability, impedance, dielectric, and electrical properties with increasing weight percents (wt.%) of silica NFs. Amid polymers, the PVDF is a semi-crystalline polymer having special features, which distinguishes it from the other polymers (Polyvinyl acetate and Poly-methyl methacrylate), and exhibits five crystalline phases (α, β, γ, δ, and ε) [5–7]. It shows enormous attention due to its outstanding properties (mechanical toughness, high dielectric constant, high flexibility, and chemical resistance) [8–10].

In this research work, the silica zinc oxide nanoparticles filled PVDF-based nanocomposite flexible sheets (PVDF-based NC FSs) are synthesized by co-precipitation method (CPM). The role of SiO_2 NFs on the synthesis of PVDF-based NC FSs having fixed amount of ZnO NFs is investigated by employing different characterization techniques, which are discussed in experimental setup.

2. Experimental Setup

The precursors [PVDF, ZnO, and silica (in powder form)] of analytical grades are used to synthesize PVDF-based NC FSs by using CPM. The average size of PVDF and NFs (SiO_2 and ZnO) is ~20 nm. Table 1 shows the wt.% of involved precursors to synthesize PVDF-based NC FSs. The different wt.% of precursors (according to Table 1) are dissolved into 15 ml solution of *N*, *N*-dimethylformamide (DMF) with magnetic stirrer at 40°C for 10 h results in the formation of uniform gels, which are further transferred to dies (dimensions: ~0.5 mm × 0.5 cm × 0.5 cm) that are placed into oven at ~45°C for 48 hours results in the formation of PVDF-based NC FSs. The FSs synthesized for different wt.% (according to Table 1) of precursors are symbolically represented by S-1, S-2, S-3, S-4, S-5, and S-6, respectively. The question is, why a fixed wt.% (10) of ZnO NFs is used in this research work? Pervaiz et al. [25] have studied the structural, optical, and dielectric properties of ZnO/PVDF-based flexible sheets, whereas the PVA-based ZnO–SiO_2 NC FSs were synthesized for fixed wt.% (5) of ZnO NFs [26]; therefore, herein, the higher wt.% (10) of ZnO NFs is used to synthesize PVDF-based Ns FSs in order to study the effect of silica NFs on the different properties of PVDF-based NC FSs containing fixed wt.% (10) of ZnO NFs.

The synthesized PVDF-based NC FSs are characterized by X-ray diffraction (XRD) [D8 ADVANCE: θ–θ X-ray diffractometer, Cu–Kα: $\lambda = 1.5406$ Å, radiation source), scanning electron microscope (SEM) [Nova NanoSEM 450 (FEI)] attached with energy-dispersive X-ray spectroscopy (EDX) , Fourier-transform infrared spectroscopy (FTIR) [TENSOR II], thermogravimetric analysis (TGA), and LCR (Precision 1910-LCR meter, QuadTech) to study the crystal structure, surface morphology, elemental compositions, weight-loss, dielectric permittivity, loss-factor, impedance, and AC conductivity, respectively. The novelty of this research work is to develop correlation between the structural, microstructural, weight-loss, dielectric permittivity, AC conductivity, and impedance of synthesized PVDF-based NC FSs as a function of increasing wt.% of silica NFs. Figure 1 illustrates the synthesis process of PVDF-based NC FSs. The detailed synthesis process of PVDF-based NC FSs by CPM can be found in literature [26].

Table 1: Wt.% of precursors used to synthesize PVDF-based NC FSs.

Sample	Solvent DMF (ml)	PVDF (wt.%)	ZnO (wt.%)	SiO_2 (wt.%)
S-1	15	100	0	0
S-2	15	90	10	0
S-3	15	85	10	5
S-4	15	80	10	10
S-5	15	75	10	15
S-6	15	70	10	20

3. Results and Discussion

3.1. Structural Analysis. Figure 2 demonstrates the XRD analysis of PVDF-based NC FSs synthesized by using CPM. A broad hump (XRD pattern of S-1) centred at 2θ values of 13.43° (ranged from 10° to 23°) corresponding to PVDF is observed, thereby indicating the formation of amorphous phase of PVDF. It has been reported that the diffraction (100), (020), and (110) planes, centred at 2θ values of 17.8°, 18.5°, and 20°, respectively, are related to PVDF phase [27]. It means that the development of broad hump, centred at 13.43° (ranged from 10° to 23°) exhibits the formation of amorphous phase of PVDF; however, its down shifting shows the existence of tensile stresses [28–30]. The XRD pattern of S-2 exhibits the development of ZnO (100), (002), (101), (102), (110), (103), and (112) planes centred at 2θ values of 32.08°, 34.67°, 35.57°, 47.845°, 56.93°, 63.19°, and 68.20°, respectively [R.C; 01-074-0534, 01-075-1533]. The intensity of diffraction planes related to ZnO phase is decreased with increasing wt.% of silica (up to 15 wt.%) NFs. Furthermore, the XRD pattern of S-3 shows the development of silica (004) and (303) planes centred at 2θ values of 43.64° and 69.43°, respectively [R.C; 01-073-0335, 01-071-0785]. The intensity of diffraction planes related to silica phase is increased with increasing wt.% of silica NFs. It means that the addition of silica NFs hinders the growth behaviour of ZnO phase, thereby indicating the creation of lattice distortion, microstrains, defects, and residual stresses [28–30]results in re-crystallize the ZnO phase. The change in crystallinity of ZnO and silica phases plays a vital role to improve the surface properties of synthesized PVDF-based NC FSs. It is interesting to note that the diffraction planes of ZnO phase are vanished for maximum wt.% of silica NFs even if all the samples contain fixed amount (10 wt.%) of ZnO NFs. This again confirms that the silica

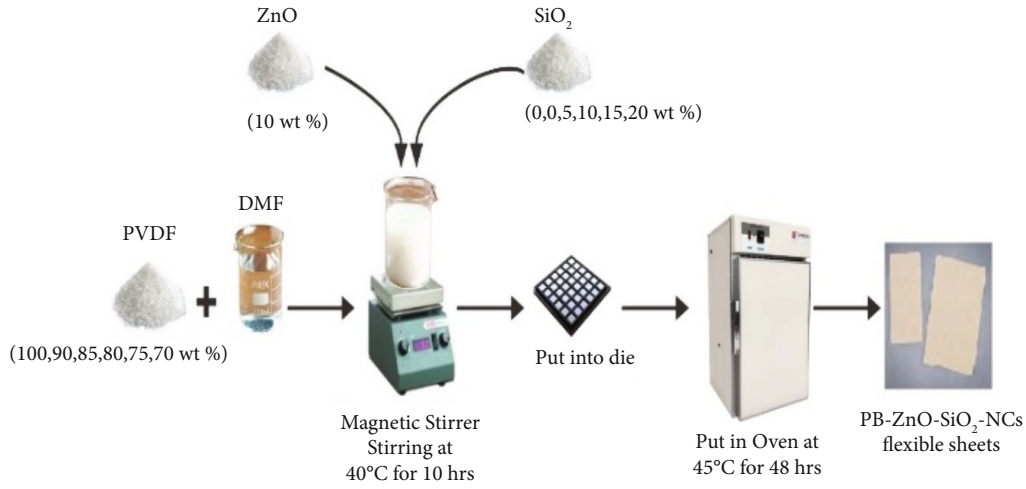

Figure 1: Schematic illustration to synthesize PVDF-based NC FSs.

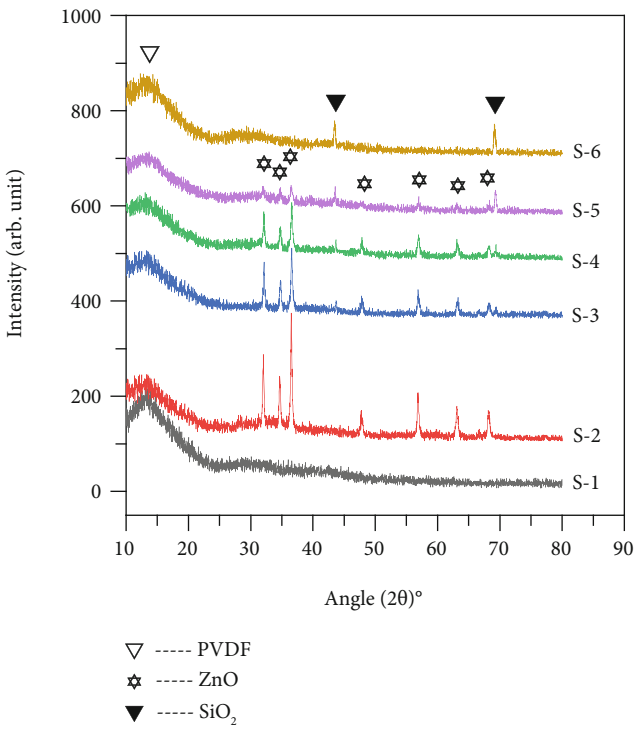

Figure 2: XRD patterns of PVDF and PVDF-based NC FSs synthesized for various wt.% of silica NFs.

NFs hinders the growth of ZnO phase results in its recrystallization. This result is agreed well with our previous report [26].

The XRD patterns of PVDF-based NC FSs exhibit that the peak intensity of various diffraction planes related to ZnO phase is decreased with increasing amount of silica NFs into PVDF matrix. It is suggested that the polycrystalline ZnO phase is encapsulated in PVDF matrix containing SiO_2 NFs results in the formation of flexible shell like complex structure around the ZnO phase. The encapsulated ZnO phase in flexible shell like complex structure could not grow, but it is decreased due to flexible shell formation around the ZnO phase whose strength is increased with increasing amount of SiO_2 NFs and, hence, causes to reduce the growth of encapsulated ZnO phase with increasing amount SiO_2 NFs. The crystallite size (CS) of ZnO (101) plane is estimated by using the relation.

$$\mathrm{CS} = \frac{k\lambda}{\mathrm{FWHM}\ \cos\theta}, \tag{1}$$

where $k = 0.89$, λ, FWHM, and θ represent the numerical constant, wavelength of incident radiation, full width half maxima, and diffraction angle, respectively [28–30]. Figure 3 exhibits the variation of CS and peak intensity of ZnO (101) plane as a function of increasing wt.% of silica NFs. The values CS and peak intensity of ZnO (101) plane are decreased with increasing amount of silica NFs. The decrease in peak intensity means decreasing crystallinity or growth of ZnO (101) plane. The decreasing growth of ZnO (101) plane is due to the formation of flexible shell like complex structure around ZnO phase in PVDF matrix. The formation of flexible shell like complex structure around ZnO phase means that it is encapsulated in flexible shell like complex structure. The decreasing CS of ZnO (101) plane means that its FWHM is increased with increasing amount of silica NFs. The decreasing behaviour of CS and peak intensity of ZnO (101) plane with increasing amount of silica NFs indicates the direct relation between CS and peak intensity; otherwise, there is no direct relation between CS and peak intensity of any diffraction plane. Additionally, the increasing FWHM of ZnO (101) plane may be due to lattice distortion created by the incorporation of silica NFs. It is notice that as the incorporation of silica NFs is increased, the lattice distortion is increased creating microstrains and defects causes to increase the FWHM and hence decrease the CS of ZnO (101) plane.

The development of broad hump related to PVDF phase and different peak intensities related to ZnO and silica phases indicates the formation of nanocrystallites, which may be separated through crystallite boundaries, which repel

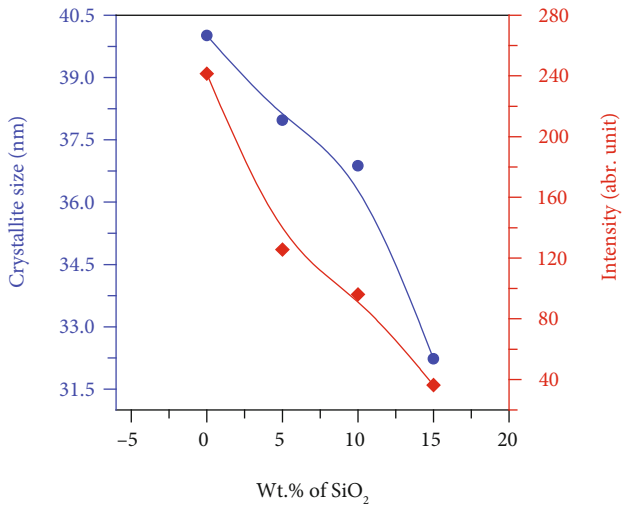

Figure 3: Variation of CS and peak intensity of ZnO (101) plane as a function of increasing of wt.% of silica NFs.

the electric field and, hence, block the charge transformation, thereby affecting the structural, microstructural, thermal, electrical, and dielectric properties. The decreasing intensity of ZnO phase is due to the formation of silica shell around the ZnO phase, hindering the growth of ZnO phase results to decrease the intensities of ZnO planes with increasing wt.% of silica NFs. In other words, the formation of polymer-based complex shell structure of silica phase hinders the growth of ZnO phase. The development of complex shell structures of polymer-based polycrystalline silica phase around ZnO NFs has already been reported in literature [24, 26–30].

3.2. SEM Analysis. Figure 4 reveals the SEM microstructures of synthesized PVDF-based NC FSs symbolically represented by S-1, S-2, S-3, S-4, S-5, and S-6. The surface morphology of S-1 shows the development of chains of pure PVDF-based agglomerates having different dimensions showing irregular distribution and seems to be embedded into PVDF matrix; however, the formation of bright and deep dark regions makes the surface rough, which may be due to non-uniform mixing of PVDF in DMF solution. The microstructure of S-2 consists of rounded NPs, which are embedded in polymer matrix; however, their distribution is uniform. A small crack is observed, which may be produced during uniform mixing of NFs into polymer and their solidifications. The microstructure of S-3 shows the formation of multilayers consisting of rounded NPs; however, the agglomeration of rounded NPs in some regions makes the surface rough. The formation of multilayers and agglomeration of NPs may be due to non-uniform mixing of polymer and NFs. This agglomerated multilayer microstructure is vanished with increasing amount of silica NFs (10 wt.%) and transferred into mesh like compact microstructure (S-4). The microstructure of S-5 shows the formation of patches of NPs; however, the different patches areas causes to make rough surface. The microstructure of S-6 shows the formation of irregular large patches separated through grain boundaries. The sizes of nanoparticles range from ~100 to −200, ~50 to 200, ~40 to 100, and ~40 to 200 nm for samples S-2, S-3, S-4, S-5, and S-6, respectively. The change in microstructures of PVDF-based NC FSs is associated with increasing wt.% of silica NFs. The growth of rounded NPs, multilayers, and irregular patches separated through grains boundaries are attributed to increasing wt.% of silica NFs. It is well known that the grains boundaries cause to block the charge transformation [26]. Figure 5 reveals the EDX spectrum of PVDF-based NC FSs (S-6) and confirms the existence of C, O, Zn, Si, and Au elements. The presence of Au is due to gold coating for SEM analysis.

3.3. FTIR Analysis. FTIR analysis is performed in order to determine the chemical bonding in PVDF-based NC FSs. Figure 6 exhibits the FTIR patterns of PVDF and PVDF-based NC FSs. The characteristic bands centred at 427 and 3280 cm^{-1} (O–Zn bond), 473 cm^{-1} (O–Si–O), 662 and 1390 cm^{-1} (α-PVDF), 1065 and 1500 cm^{-1} (Si–O–Si), 1098 cm^{-1} (Si–O), 1265 cm^{-1} (β-PVDF), 1644 and 2993–3611 cm^{-1} ($ZnO–SiO_2$), and 2360 cm^{-1} (Si–C) indicate the formation of chemical bonds between the newly formed compounds. This result is agreed well with the reported literature [23, 31–37]. The characteristic band centred at 1644 cm^{-1} is related to O–H bending vibrational mode, whereas a broad band ranging from 2993 to 3611 cm^{-1} indicates the presence of O–H stretching vibrational mode of $ZnO–SiO_2$ compound. The characteristic band centred at 662, 1390, and 1265 cm^{-1} is related to various phases of PVDF.

It is obvious that the intensity of above mentioned bands related to PVDF and PVDF-based NC FSs is increased up to 15 wt.% of silica NFs. It is known that the increase in band intensity indicates the increasing strength of chemical bonds.

It is known that the shifting of FTIR band towards lower wavenumber indicates the increase of reduced mass. In this case, no significant shifting of FTIR band indicates that the reduced mass remains constant; however, the intensities and broadening of FTIR bands are increased with increasing amount of silica NFs. The increasing intensity of FTIR bands indicates the increasing strength of chemical bonds. The broadening of FTIR bands is responsible to create microstrains and defects and, hence, develops microstresses. In short, the higher the intensity of FTIR bands, the greater will be the bond strength, whereas the increasing broadening indicates the development of microstrains and defects and, hence, caused to produce microstresses in the synthesized PVDF-based NC FSs. We have already mentioned that the ZnO NFs are encapsulated into polymer-based SiO_2 shell structure, which hinders the growth of ZnO phase (XRD analysis). It is interesting to note that, for 20 wt% of silica NFs, the weak intensity of all vibration bands related to various compounds is due to larger contents of silica NFs. This result is agreed well with the XRD analysis. Additionally, the development of several vibrational bands indicates the formation of complicated network of chemical bonding. The

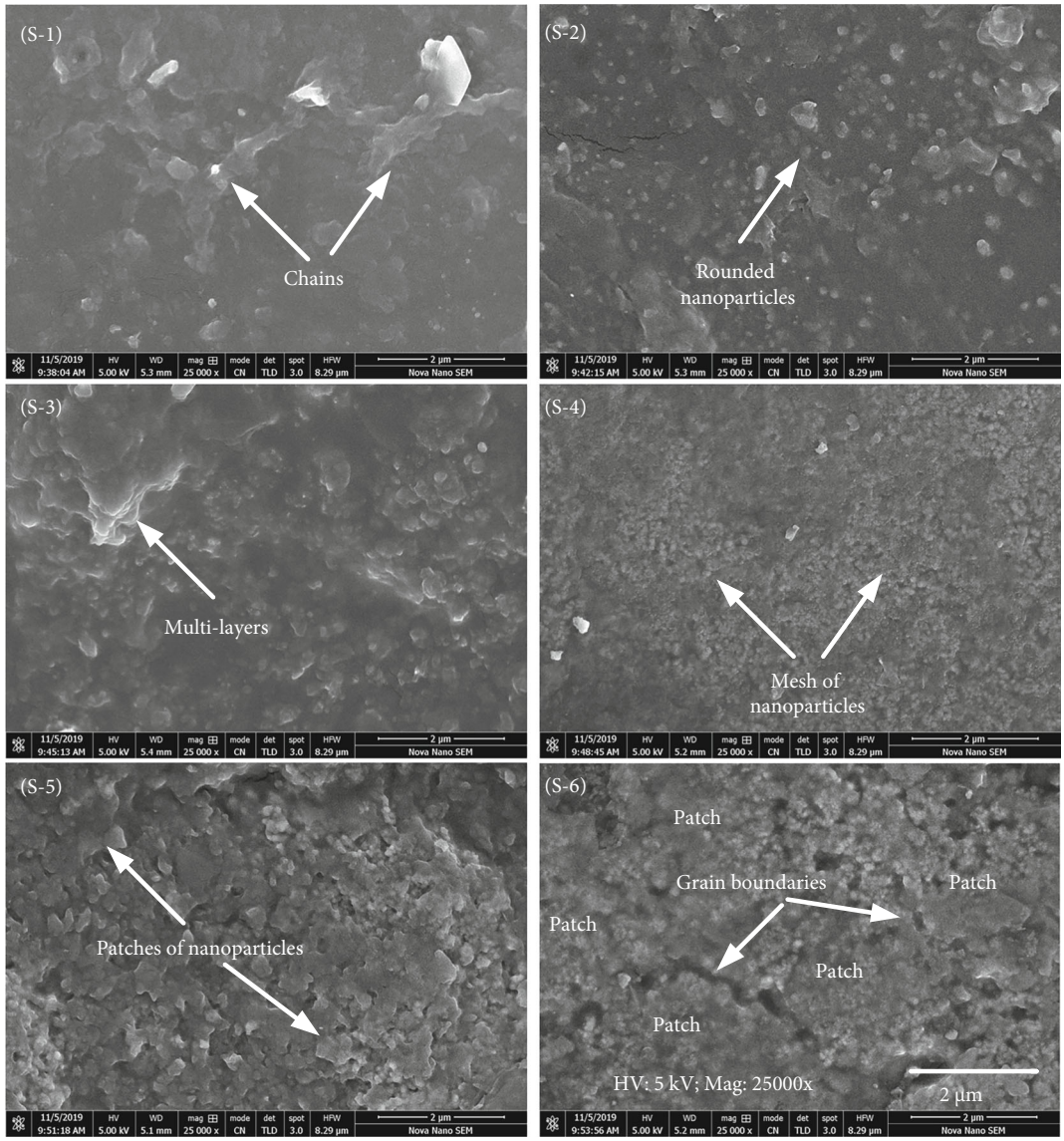

Figure 4: SEM microstructures of PVDF and PVDF-based NC FSs synthesized for various wt.% of silica NFs.

coexistence of various compounds inside the PVDF-based NC FSs may causes to enhance the dielectric properties.

3.4. Thermal Stability. The thermal stability of PVDF and PVDF-based NC FSs is studied by TGA analysis. Figure 7 exhibits the variation of wt. loss (%) of PVDF and PVDF-based NC FSs. Table 2 shows the fractional change in wt. loss (%) of PVDF-based NC FSs along with PVDF at different temperatures. The wt. loss (%) of PVDF-based NC FSs is divided into three regions.

The PVDF FSs (S-1) experienced the first weight loss (~1.42 wt.%) at temperature ~100°C. The major wt loss (%) of all synthesized PVDF-based NC FSs occurred in the temperature range of ~260°C to 400°C. At temperature below ~260°C, the wt. loss (%) of S-1, S-2, S-4, and S-5 is found to be ~5.8%, whereas it is found to be 8.4, 2.4% for S-3 and S-6, respectively. The wt loss (%) of S-3 is significantly higher, which is due to the addition of (5 wt.%) silica NFs. Actually, the wt loss (%) is due to the breaking of physically weak and chemically strong bonds and, hence, partially evaporated, results in the formation of PVDF-based NC FSs holding NFs [38]. The main dramatic wt. loss (%) observed in temperature range (~260°C to 400°C) is due to the degradation of side-chain of polymer, NFs, and their mutual interactions [23]. At temperature above 450°C, the wt loss (%) of S-2 begins to decrease slightly as compared to S-1, whereas it begins to decrease promptly of S-3, S-4, S-5, and S-6 with increasing wt.% of silica NFs. This decreasing wt loss (%) of PVDF-based NC FSs indicates that the type and amount of NFs act as heat absorption barriers and, hence, are responsible to improve the thermal stability at high temperature [23]. We have already discussed that with increasing silica NFs, the crystallinity of ZnO phase is decreased, whereas it is increased for silica

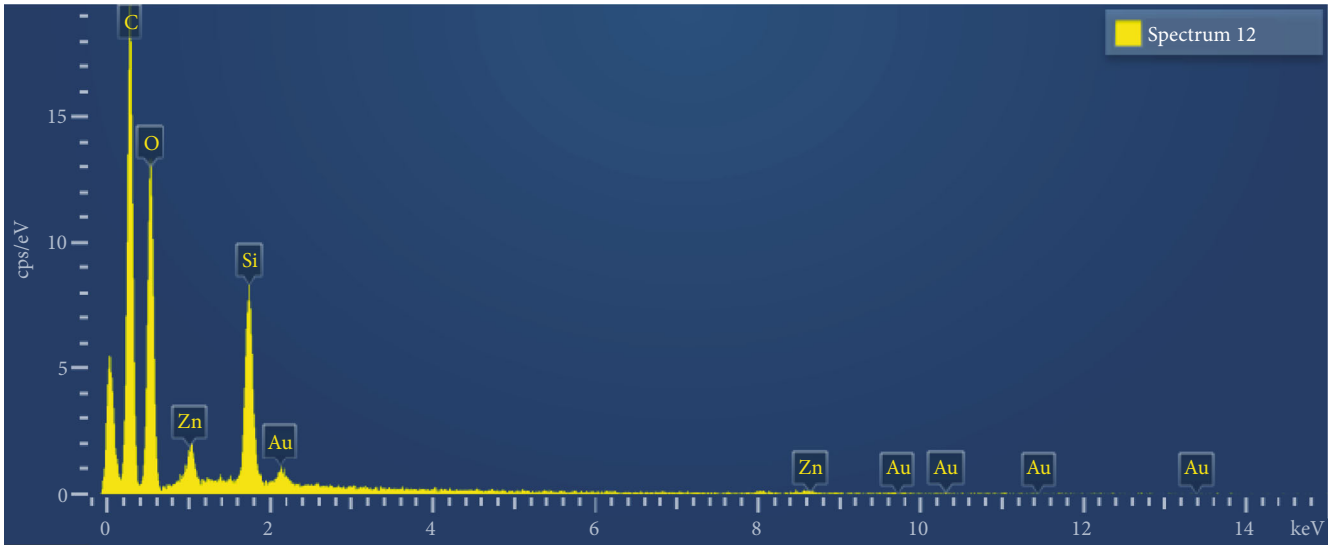

Figure 5: Typical EDX spectrum of PVDF-based NC FSs with 20 wt.% silica NFs.

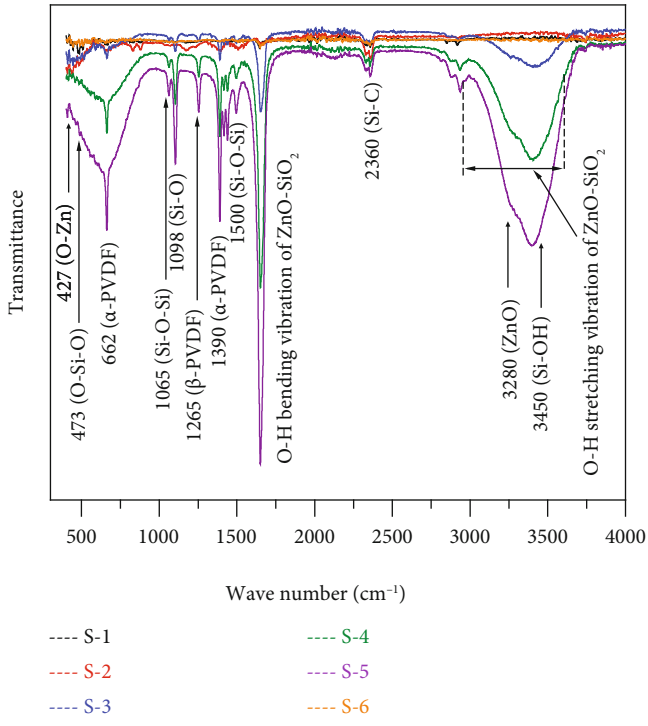

Figure 6: FTIR spectra of PVDF and PVDF-based NC FSs.

phase (XRD analysis). The change in structural parameters is responsible to change the microstructures, chemical bonding, as well as the dramatic wt loss (%) of PVDF-based NC FSs with increasing NFs responsible to increase the thermal stability of synthesized samples at high temperature.

3.5. Dielectric Analysis. The dielectric parameter of synthesized PVDF-based NC FSs with increasing frequency is defined by complex dielectric permittivity comprising two factors (dielectric constant = ε' and dielectric loss = ε''), which are linked by the following relation.

$$\varepsilon^* = \varepsilon' - j\varepsilon'', \tag{2}$$

where j is constant. Additionally, the ε' and ε'' represent the energy storage and energy loss during each cycle of applied electric field, respectively. The values of ε' and ε'' are calculated from the following relations

$$\varepsilon' = \frac{Cd}{(A\varepsilon_o)}, \tag{3}$$

$$\varepsilon'' = \varepsilon' \text{ (loss factor)}, \tag{4}$$

where C is the capacitance, d is the thickness, A is thesurface area, and ε_0 is the permittivity of free space (8.854×10^{-12} F/m). The permittivity of PVDF-based NC FSs is estimated by using dielectric polarization mechanism, which may be related to the constituents (PVDF, ZnO, and silica) of PVDF-based NC FSs as well as the interfacial areas between PVDF matrix and NFs [39].

Figure 8 reveals the variation in ε', ε'', loss factor ($\tan\delta$), and AC conductivity (σ_{ac}) of synthesized PVDF-based NC FSs with increasing frequency and wt.% of NFs, respectively. Figure 8(a) exhibits the variation in ε' values of PVDF-based NC FSs with increasing frequency and wt.% of NFs. The values of ε' are decreased sharply/slowly in low/high frequency regions, which is due to intrinsic characteristics of ZnO NPs [40, 41]. Therefore, the coexistence of (ZnO and silica) NFs into polymer matrix may cause to reduce the values of ε' with increasing frequency. The value of ε' for PVDF-based NC FSs containing fixed amount (10 wt.%) of ZnO NFs is increased significantly; however, the values of ε' are further increased with increasing amount (5, 10, 15, and 20 wt.%) of silica NFs. Additionally, the values of ε' for S-1, S-2, and S-3 are found to be 2.68, 5.51, and 8.76, respectively. The values of ε' are further increased from 8.76 to

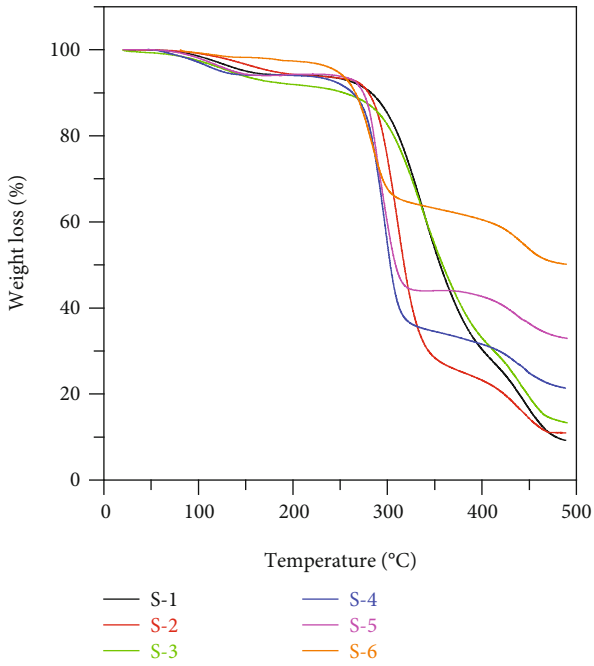

Figure 7: Variation in wt loss (%) of PVDF and PVDF-based NC FSs.

Table 2: Fractional change in wt. loss (%) of synthesized PVDF and PVDF-based NC FSs.

Sample	Wt loss (%) with increasing temperature (°C)							
	100	150	200	250	300	350	400	450
S-1	1.42	4.27	5.79	6.44	14.94	44.20	70.09	83.85
S-2	1.33	3.36	5.38	6.84	25.05	70.90	76.97	85.87
S-3	1.74	6.19	8.21	9.68	17.77	42.98	67.26	80.61
S-4	2.50	6.17	6.19	8.06	45.69	65.24	68.88	75.35
S-5	2.14	5.79	5.79	6.03	41.64	56.33	57.55	64.02
S-6	0.93	1.74	2.55	5.63	32.34	36.91	39.74	46.62

13.71 with increasing amount (5–20 wt%) of silica NFs, respectively. Moreover, the values of ε' for PVDF-based NC FSs are decreased with increasing frequency, which is due to the existence of dipoles that align themselves along the applied field [39]; however, it is difficult for larger dipoles to align themselves at higher frequencies. The parameters that may effect on the values of ε' for PVDF-based NC FSs are the size and number density of dipole as well as interactions between them. It is well known that the high value of ε' for PVDF-based NC FSs in low frequency region is mainly due to electrode as well as sample interfacial effects [42]. Moreover, the values of ε' for PVDF-based NC FSs are decreased with increasing frequency because the permittivity of ZnO has inverse relation with frequency [43, 44]. Figure 8(b) demonstrates that the values of ε'' for PVDF-based NC FSs are decreased abruptly in low frequency region because the dipoles have sufficient time to align themselves; however, the values of ε'' are decreased gradually because the dipoles have insufficient time in high frequency region to align themselves along the applied field [39]. It has been reported that the dielectric loss is associated with the following factors: O–H groups and bonding between O–H and H, which are responsible to improve/change the structure, microstructure, and electrical, thermal, and dielectric properties of synthesized PVDF-based NC FSs [5]. The increasing amount of NFs (ZnO and silica) may be the other reason to improve the said properties. This statement is agreed well with the XRD, FTIR, SEM, and thermal analysis.

Figure 8(c) exhibits the variation of loss factor of synthesized PVDF-based NC FSs with increasing frequency. The loss factor is decreased abruptly in low frequency region, whereas it is decreased slowly in high frequency region. Moreover, the loss factor is decreased significantly with increasing amount of silica NFs because on applying electric field, the NFs tend to block the electric current in polymer matrix, and therefore, no electrical energy is changed into thermal energy [26].

Figure 8(d) shows the variation of AC conductivity (σ_{ac}) of PVDF-based NC FSs with increasing frequency, and the values of σ_{ac} for PVDF-based NC FSs are calculated by using the following relation.

$$\sigma_{ac} = \varepsilon_0 \varepsilon' \omega(\tan \delta), \tag{5}$$

where $\omega = 2\pi f$ and $\tan\delta$ is the loss-factor. It is obvious that the values of σ_{ac} are increased exponentially with increasing frequency and wt.% of NFs. The deep investigation reveals that the values of σ_{ac} are increased significantly with increasing frequency even in low frequency region. Moreover, the σ_{ac} of PVDF-based NC FSs does not depend on applied field and scattering in low frequency region. This statement holds for disordered materials and can be described by the following equation.

$$\sigma(\omega) = \sigma_o + A\omega^n, \tag{6}$$

where σ_o, A, and n indicate the DC-conductivity, pre-exponential, and fractional exponent, respectively. The smaller values of σ_{ac} (in low frequency region) are due to electrode polarization [5], whereas in high frequency region, microstrains and point-defects are created due to electronic interaction between polymer and NFs results in grain boundaries formation (SEM analysis). Additionally, deep investigation reveals that the values of σ_{ac} are increased significantly with increasing frequency even in low frequency region. However, the formation of microstrains, point defects, formation of multilayers, mesh, and patches like microstructures separated through grain boundaries in the synthesized PVDF-based NCs FSs are increased progressively with increasing wt.% of silica NFs. It is known that an electronic communication process is produced in the synthesized PVDF-based NC FSs, which reduces the degree of crystallinity and, hence, increases the amorphous nature of synthesized PVDF-based NC FSs. The amorphous region in the synthesized PVDF-based NC FSs is increased progressively with increasing frequency. Thus, in amorphous region, the polymer chain attains faster interior modes in which bond rotations create segmental motion, which in turn makes the polymer chains

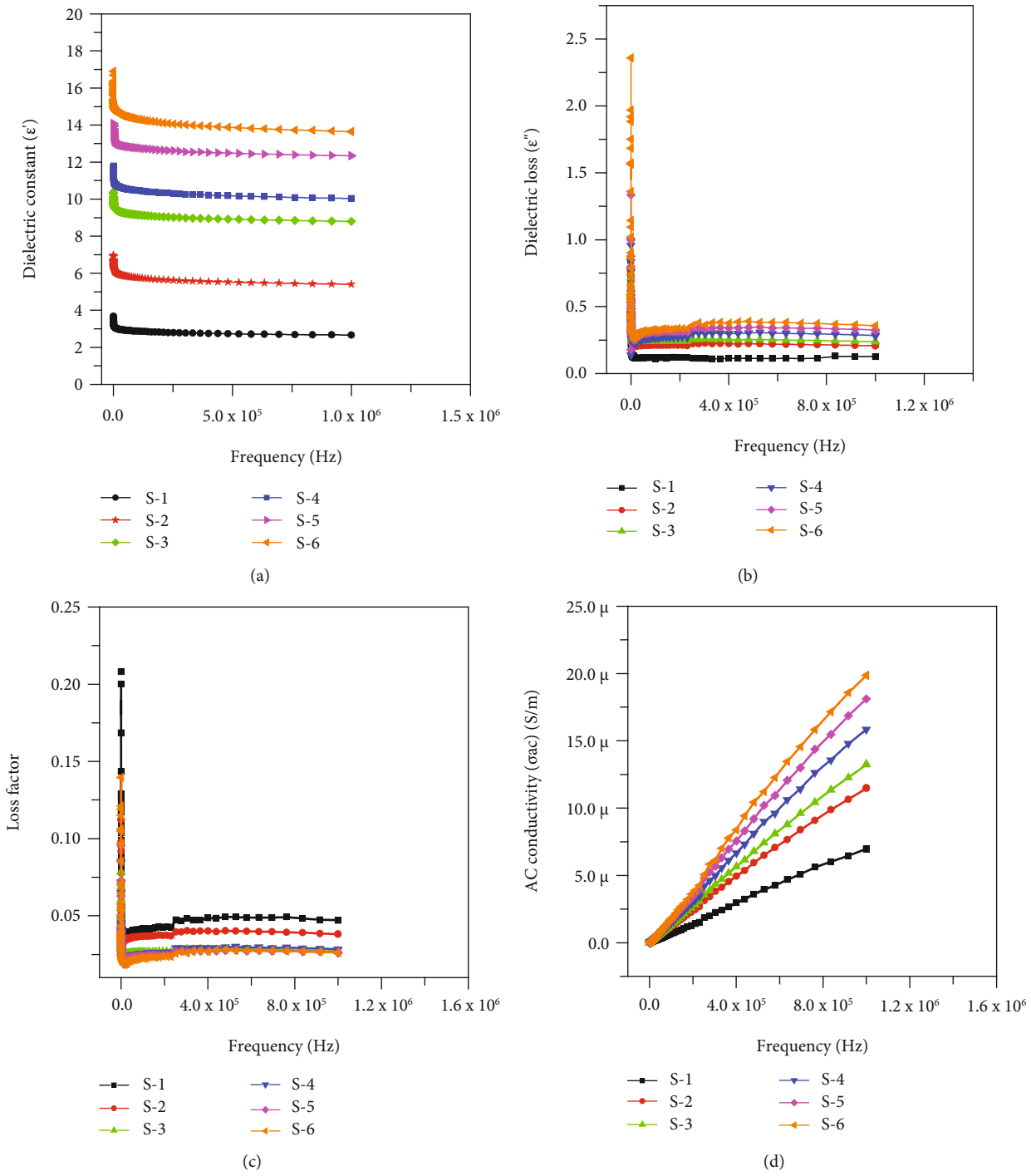

FIGURE 8: Variation in the values of (a) ε', (b) ε'', (c) tan δ, and (d) σ_{ac} of PVDF and PVDF-based NC FSs with increasing frequency and wt.% of silica NFs, respectively.

more flexible and, hence, increases the conductivity of PVDF-based NC FSs. Such type of segmental motion and chain of PVDF matrix are produced due to microstrains, point defects, and encapsulated microstructures linked with increasing amount of silica NFs, making the PVDF-based NC FSs more flexible, strong, and conductive. Results show that the synthesized flexible sheets of PVDF-based NC FSs can be used as flexible semiconducting materials for the manufacturing of many flexible electronic devices. Therefore, such segmental motion is responsible to enhance the σ_{ac} of synthesized PVDF-based NC FSs. Moreover, the segmental motion is increased with increasing wt.% of NFs. It means that the σ_{ac} of PVDF-based NC FSs is increased with increasing wt.% of NFs. The σ_{ac} of S-6 is found to be 19.92 $\times 10^{-6}$ S/m, which is three times higher than S-1. Nasir et al. [45] have reported that the electrical conduction

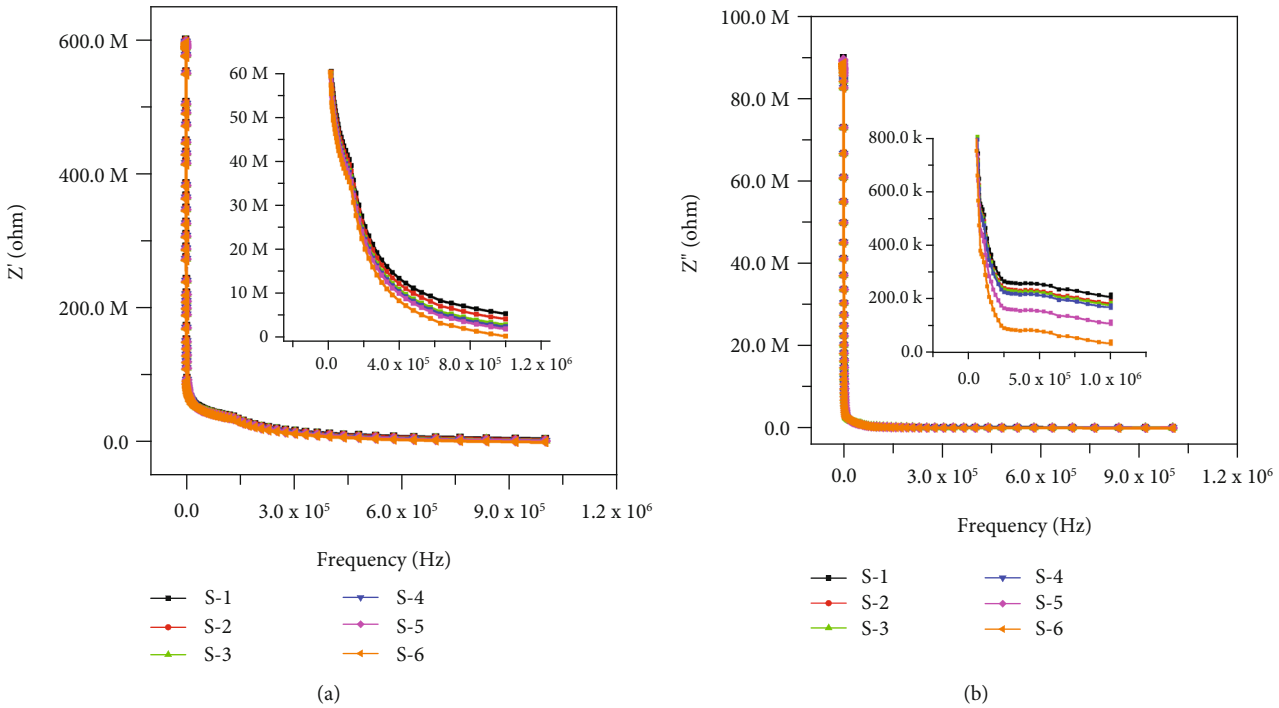

Figure 9: Variation in Z' (a) and Z'' (b) of synthesized PVDF and PVDF-based NC FSs with increasing frequency.

Table 3: Comprehensive review of various parameters of synthesized PVDF and PVDF-based NC FSs.

Sample	Structure	Morphology	Wt. loss (%) [<450°C]	ε'	ε''	Loss factor	$Z \times 10^6$ (Ω) Z'	Z''	$\sigma_{ac\times10}{}^{-6}$ (S/m)
S-1	Hump of PVDF	Chains	90.42	2.68	0.13	0.047	5.4	0.21	6.69
S-2	Polycrystalline	Rounded NPs	88.69	5.51	0.21	0.039	4.2	0.20	11.51
S-3	Polycrystalline	Multilayers	86.50	8.76	0.23	0.029	3.4	0.19	13.22
S-4	Polycrystalline	Mesh of NPs	78.72	10.03	0.28	0.027	2.6	0.17	15.81
S-5	Polycrystalline	Patches of NPs	66.61	12.44	0.32	0.026	1.9	0.11	18.21
S-6	Polycrystalline	Large patches isolated by grain boundaries	49.32	13.71	0.36	0.025	0.16	0.037	19.92

mechanism is related to the electrons and polaron hopping mechanism, which can act as hopping channels. The increasing frequency of applied field facilitates the conductive channels and, hence, promotes the hopping of charge carriers. Therefore, the increasing values of σ_{ac} are due to conduction mechanism, which may occur due to polaron hopping mechanism.

The complex impedance (Z^*) is employed to investigate the electrical conduction mechanism in poly-crystalline materials. The Z^* consists of Z' (real) and Z'' (imaginary) parts, which are correlated with each other through the following equation.

$$Z^* = Z' + jZ'', \tag{7}$$

$$Z' = Z\cos\theta, \tag{8}$$

$$Z'' = Z\sin\theta. \tag{9}$$

Figure 9 shows the variation of Z' (Figure 9(a)) and Z'' (Figure 9(b)) of PVDF-based NC FSs with increasing frequency. The values of Z' are decreased sharply in low frequency region, whereas it seems to be frequency independent in high frequency region (low magnified version of Figure 9(a)). Careful investigation (magnified version of Figure 9(a)) reveals that the values of Z' are exponentially decreased with increasing frequency, whereas these values are decreased significantly with increasing amount of silica NFs (magnified version of Figure 9(a)) in the synthesized PVDF-based NC FSs.

In our case, the values of Z' (Figure 9(a)) of PVDF-based NC FSs are decreased gradually with increasing frequency and wt.% of silica NFs. It means that the values of Z' depend on wt.% of NFs and frequency in high frequency region. This decreasing value of Z' of PVDF-based NC FSs with increasing wt.% of silica NFs causes to increase the σ_{ac} of PVDF-based NC FSs (already discussed). A similar behaviour in the variation of Z'' (Figure 9(b)) of PVDF-based NC FSs with increasing frequency and wt.% of silica NFs is observed. Therefore, in the synthesized PVDF-based NC FSs, a continuous conductive network has started by

increasing frequency and wt.% of silica NFs through the creation of non-trapped charge particle whose concentration is increased with increasing wt.% of silica NFs, and hence, the non-trapped charge particles are responsible to increase the conducting behaviour of PVDF-based NC FSs.

We have already mentioned that the increasing frequency facilitates the conductive channels, promoting the hopping of charge carrier's results in the increase of conductivity. The concentration of such charge carriers is also increased with increasing wt.% of silica NFs, which increases the conductivity and, hence, reduces the impedance of PVDF-based NC FSs. Moreover, the formation of NPs of various microstructures plays an important role for exciting electrons significantly so that they can hop from one conducting cluster (comprising of NPs) to another due to smaller interparticle gaps [46]. This leads to decrease the impedance and increase in conductivity of PVDF-based NC FSs. The synthesized PVDF-based NC FSs having maximum wt.% of silica NFs significantly affect the impedance and conductivity. Table 3 demonstrates the comprehensive review of various properties and their change with increasing wt.% of silica NFs in PVDF-based NC FSs.

4. Conclusions

This research work inferred the effect of silica NFs on different properties of PVDF-based NC FSs having fixed wt.% of ZnO NFs. Such PVDF-based NC FSs growing along ZnO (100), (002), and (101) and SiO_2 (004) and (303) planes are successfully synthesized by CPM. The crystallinity of ZnO phase is reduced with increasing wt.% of silica NFs. The increasing wt.% of silica hinders the growth of ZnO phase in polymer matrix. The microstructures of synthesized PVDF-based NC FSs (having fixed amount of ZnO NFs) are changed with increasing wt.% of silica NFs. The chemical bonding between the involved precursors is confirmed through FTIR analysis. At high temperature, the wt. loss (%) of S-1 (89.90%) is reduced to 49.26% (S-6) with increasing wt.% of silica NFs. For S-6, the estimated values of dielectric permittivity, loss-factor, impedance, and AC conductivity of S-6 are found to be 13.7, 0.03, 0.16 MΩ, and 19.9×10^{-6} S/m, respectively, which are 5.1, 0.5, 0.03, and 2.9 times than S-1, respectively. The change in crystal structures, microstructures, thermal, electrical, and dielectric properties of all synthesized PVDF-based NC FSs is linked with defects, microstrains, and capsulated microstructure arising during the synthesis process and, hence, is responsible to generate segmental motion, which makes the synthesized NCs more flexible, conductive, and strong. Hence, the synthesized PVDF-based NC FSs may be used as flexible semiconductors for optoelectronic devices, light emitting diodes, and energy storage applications.

Data Availability

The supporting data related to this research article will be available from the corresponding author on reasonable request.

Conflicts of Interest

The author(s) declare(s) that they have no conflicts of interest.

Acknowledgments

This research work is self-supported; however, the authors are grateful to Dr. Adnan Ali for characterizations.

References

[1] L. L. Beecroft and C. K. Ober, "Nanocomposite materials for optical applications," *Chemistry of Materials*, vol. 9, no. 6, pp. 1302–1317, 1997.

[2] R. V. Kumar, R. Elgamiel, Y. Diamant, and A. Gedanken, "Sonochemical preparation and characterization of nanocrystalline copper oxide embedded in poly(vinyl alcohol) and its effect on crystal growth of copper oxide," *Langmuir*, vol. 17, no. 2001, pp. 1406–1410, 2001.

[3] D. R. Denison, J. C. Barbour, and J. H. Burkart, "Low dielectric constant, fluorine-doped SiO_2 for intermetal dielectric," *Journal of Vacuum Science & Technology*, vol. 14, no. 3, pp. 1124–1126, 1996.

[4] M. Tada, Y. Harada, K. Hijioka et al., "Cu dual damascene interconnects in porous organosilica film with organic hardmask and etch-stop layers for 70 nm-node ULSIs," *IEEE International Interconnect Technology Conference*, pp. 12–14, 2002.

[5] S. H. Rashmi, A. Raizada, G. M. Madhu, A. A. Kittur, R. Suresh, and H. K. Sudhina, "Influence of zinc oxide nanoparticles on structural and electrical properties of polyvinyl alcohol films," *Plastics, Rubber and Composites*, vol. 44, no. 1, pp. 33–39, 2015.

[6] P. K. C. Pillai, G. K. Narula, and A. K. Tripathi, "Dielectric properties of polypropylene/polycarbonate polyblends," *Polymer Journal*, vol. 16, no. 7, pp. 575–578, 1984.

[7] A. K. Batra, P. Guggilla, D. Cunningham, M. D. Aggarwal, and R. B. Lal, "Growth and characterization of rare earths doped triglycine sulfate crystals," *Physica B: Condensed Matter*, vol. 371, no. 2, pp. 210–214, 2006.

[8] A. J. J. Manoharan, N. J. John, V. Revathi, K. V. Rajendran, and P. M. Andavan, "Effect of amino acid doping on the dielectric properties of triglycine sulphate (TGS) crystals," *Indian Journal of Science and Technology*, vol. 4, no. 6, pp. 688–692, 2011, ISSN: 0974-684.

[9] N. Kartheeswari and K. Viswanathan, "Vibrational spectral studies of pure and doped TGSP crystals," *Journal of Spectroscopy*, vol. 2013, p. 12, 2013.

[10] C. Shao, H. Y. Kim, J. Gong et al., "Fiber mats of polyvinyl alcohol/silica composite via electrospinning," *Materials Letters*, vol. 57, no. 9–10, pp. 1579–1584, 2003.

[11] V. Goodship and D. Jacobs, *Polyvinyl Alcohol: Materials, Processing and Applications*, vol. 16, UK Rapra Review Report, Smithers Rapra Technology, 2009, http://www.bookdepository.co.uk/Polyvinyl-Alcohol.

[12] M. Krumova, D. Lopez, R. Benavente, C. J. M. Mijangos, and J. M. Pereña, "Effect of crosslinking on the mechanical and thermal properties of poly(vinyl alcohol)," *Polymer*, vol. 41, no. 26, pp. 9265–9272, 2000.

[13] S. Sathish, B. C. Chandar, and B. T. Bhavyasree, "Nano composite PVA-TiO_2 thin films for OTFTs," *Journal: Advanced Materials Research*, vol. 678, pp. 335–342, 2013.

[14] S. D. Korlann, A. E. Riley, B. L. Kirsch, B. S. Mun, and S. H. Tolbert, "Chemical tuning of the electronic properties in a periodic surfactant-templated nanostructured semiconductor," *Journal of the American Chemical Society*, vol. 127, no. 36, pp. 12516–12527, 2005.

[15] B. S. Zou, R. Liu, F. Wang, A. Pan, L. Cao, and Z. L. Wang, "Lasing mechanism of ZnO nanowires/nanobelts at room temperature," *The Journal of Physical Chemistry. B*, vol. 110, no. 26, pp. 12865–12873, 2006.

[16] J. I. Hong, P. Winberg, L. S. Schadler, and R. W. Siegel, "Dielectric properties of zinc oxide/low density polyethylene nanocomposites," *Materials Letters*, vol. 59, no. 4, pp. 473–476, 2005.

[17] S. C. Tjong, G. D. Liang, and S. P. Bao, "Electrical properties of low-density polyethylene/ZnO nanocomposites: the effect of thermal treatments," *Journal of Applied Polymer Science*, vol. 102, no. 2, pp. 1436–1444, 2006.

[18] H. Gleiter, J. Weissmuller, O. Wollersheim, and R. Würschum, "Nanocrystalline materials: away to solids with tunable electronic structures and properties," *Acta Materialia*, vol. 49, no. 4, pp. 737–745, 2001.

[19] J. Moczo and B. Pukanszky, "Polymer micro and nanocomposites: structure, interactions, properties," *Journal of Industrial and Engineering Chemistry*, vol. 14, no. 5, pp. 535–563, 2008.

[20] H. Zou, S. Wu, and J. Shen, "Polymer/silica nanocomposites: preparation, characterization, properties, and applications," *Chemical Reviews*, vol. 108, no. 9, pp. 3893–3957, 2008.

[21] A. M. D. Pascual, M. A. G. Fatou, F. Ania, and A. Flores, "Nanoindentation in polymer nanocomposites," *Progress in Materials Science*, vol. 67, pp. 1–94, 2015.

[22] N. Dispat, S. Poompradub, and S. Kiatkamjornwong, "Synthesis of ZnO/SiO_2-modified starch-graft-polyacrylate superabsorbent polymer for agricultural application," *Carbohydrate Polymers*, vol. 249, p. 116862, 2020.

[23] X. Liu, X. Chen, J. Ren, M. Chang, B. He, and C. Zhang, "Effects of nano-ZnO and nano-SiO_2 particles on properties of PVA/xylan composite films," *International Journal of Biological Macromolecules*, vol. 132, pp. 978–986, 2019.

[24] X. J. Huang, X. F. Zeng, J. X. Wang, L.-I. Zhang, and J. Chen, "Synthesis of monodispersed ZnO@SiO_2 nanoparticles for anti-UV aging application in highly transparent polymer-based nanocomposites," *Journal of Materials Science*, vol. 54, no. 11, pp. 8581–8590, 2019.

[25] S. Pervaiz, N. Kanwal, S. A. Hussain, M. Saleem, and I. A. Khan, "Study of structural, optical and dielectric properties of ZnO/PVDF-based flexible sheets," *Journal of Polymer Research*, vol. 28, no. 8, pp. 309–322, 2021.

[26] S. Pervaiz, I. A. Khan, S. A. Hussain, N. Kanwal, A. Farid, and M. Saleem, "Polymer based ZnO–SiO_2 nanocomposite flexible sheets as high dielectric materials," *Journal of Inorganic and Organometallic Polymers and Materials*, vol. 31, pp. 209–219, 2020.

[27] K. S. Tan, W. C. Gan, T. S. Velayutham, and W. H. A. Majid, "Pyroelectricity enhancement of PVDF nanocomposite thin films doped with ZnO nanoparticles," *Journal of Smart Materials and Structures*, vol. 23, no. 12, p. 125006, 2014.

[28] R. Ahmad, T. Hussain, I. A. Khan, and R. S. Rawat, "Synthesis of ZrSiN composite films using a plasma focus device," *Chinese Physics B*, vol. 23, no. 6, article 065204, 2014.

[29] S. Jabbar, I. A. Khan, R. Ahmad, M. Zakaullah, and J. S. Pan, "Carbonitriding of silicon using plasma focus device," *Journal of Vacuum Science and Technology A*, vol. 27, no. 2, pp. 381–387, 2009.

[30] I. A. Khan, R. S. Rawat, R. Ahmad, and M. A. K. Shahid, "Post-annealing effect on the structural and mechanical properties of multiphase zirconia films deposited by a plasma focus device," *Chinese Physics B*, vol. 22, no. 12, p. 127306, 2013.

[31] J. V. G. Tinio, K. T. Simfroso, A. D. M. V. Peguit, and R. T. C. Candidato Jr., "Influence of OH^- ion concentration on the surface morphology of ZnO–SiO_2 nanostructure," *Journal of Nanotechnology*, vol. 2015, p. 7, 2015.

[32] I. M. Joni, L. Nulhakim, M. Vanitha, and C. Panatarani, "Characteristics of crystalline silica (SiO_2) particles prepared by simple solution method using sodium silicate (Na_2SiO_3) precursor," *Journal of Physics: Conference Series*, vol. 1080, pp. 1–6, 2018.

[33] B. Li and H. Cao, "ZnO@graphene composite with enhanced performance for the removal of dye from water," *Journal of Materials Chemistry*, vol. 21, pp. 3346–3349, 2011.

[34] V. Bansal, D. Rautaray, A. Bharde et al., "Fungus-mediated biosynthesis of silica and titania particles," *Journal of Materials Chemistry*, vol. 15, no. 26, pp. 2583–2589, 2005.

[35] B. H. Patel and P. N. Patel, "Synthesis and characterization of silica nanoparticles by acid leaching technique," *Research Journal of Chemical Sciences*, vol. 4, pp. 52–55, 2014.

[36] U. Kalapathy, A. Proctor, and J. Shultz, "An improved method for production of silica from rice hull ash," *Bioresource Technology*, vol. 85, no. 3, pp. 285–289, 2002.

[37] E. Moncada, R. Quijada, and J. Retuert, "Nanoparticles prepared by the sol-gel method and their use in the formation of nanocomposites with polypropylene," *Nanotechnology*, vol. 18, no. 33, p. 335606, 2007.

[38] V. M. Nikolic, D. L. Zugic, A. D. Maksic, D. P. Saponji, and M. P. M. Kaninski, "Performance comparison of modified poly(vinyl alcohol) based membranes in alkaline fuel cells," *International Journal of Hydrogen Energy*, vol. 36, no. 17, pp. 11004–11010, 2011.

[39] P. Dutta, S. Biswas, and S. K. De, "Dielectric relaxation in polyaniline–polyvinyl alcohol composites," *Materials Research Bulletin*, vol. 37, no. 1, pp. 193–200, 2002.

[40] T. Tanaka, "Dielectric nanocomposites with insulating properties," *IEEE Transactions on Dielectrics and Electrical Insulation*, vol. 12, no. 5, pp. 914–928, 2005.

[41] Y. Cao, P. C. Irwin, and K. Younsi, "The future of nanodielectrics in the electrical power industry," *IEEE Transactions on Dielectrics and Electrical Insulation*, vol. 11, no. 5, pp. 797–807, 2004.

[42] R. Singh, R. T. Tandon, V. S. Panwar, and S. Chandra, "Low frequency ac conduction in lightly doped poly-pyrrole films," *Journal of Applied Physics*, vol. 69, no. 4, pp. 2504–2511, 1991.

[43] A. Livi, V. Levita, and P. A. Rolla, "Dielectric behavior at microwave frequencies of an epoxy resin during crosslinking," *Journal of Applied Polymer Science*, vol. 50, no. 9, pp. 1583–1590, 1993.

[44] J. P. Eloundou, "Dipolar relaxations in an epoxy-amine system," *European Polymer Journal*, vol. 38, no. 3, pp. 431–438, 2002.

[45] S. Nasir, G. Asghar, M. A. Malik, and M. A. Rehman, "Structural, dielectric and electrical properties of zinc doped nickel nano-ferrites prepared by simplified sol–gel method," *Journal of Sol-Gel Science and Technology*, vol. 59, no. 1, pp. 111–116, 2011.

[46] L. Nayak, D. Khastgir, and T. K. Chaki, "Study of alternating current impedance analysis and dielectric properties of carbon nanotube-based polysulfone nanocomposites," *Polymer Composites*, vol. 33, no. 1, pp. 85–91, 2012.